Hindawi
Journal of Food Biochemistry
Volume 2024, Article ID 5552747, 13 pages
https://doi.org/10.1155/2024/5552747

Research Article

Sophora japonica Extract Inhibits Ulcerative Colitis and Colitis-Associated Colon Cancer via Regulation of Lipid Metabolism

Ying Zheng,[1,2,3] **Tianjiao Li**,[1,2,3] **Xi Luo**,[1] **Mengnan Jia**,[1] **Liying Han**,[1] **Hao Yu**,[1] **Yongrui Bao**,[1,2,3] **Shuai Wang**,[1,2,3] **and Xiansheng Meng**[1,2,3]

[1]*College of Pharmacy, Liaoning University of Traditional Chinese Medicine, Dalian 116600, China*
[2]*Liaoning Multi-Dimensional Analysis of Traditional Chinese Medicine Technical Innovation Center, Dalian 116600, China*
[3]*Liaoning Province Modern Traditional Chinese Medicine Research and Engineering Laboratory, Dalian 116600, China*

Correspondence should be addressed to Xiansheng Meng; mxsvvv@126.com

Received 1 April 2023; Revised 30 January 2024; Accepted 4 March 2024; Published 19 March 2024

Academic Editor: Ramachandran Srinivasan

Inflammation is a well-known risk factor for tumor development. Intervening in chronic inflammation may be an effective approach to inhibit the progression of ulcerative colitis (UC) to colitis-associated colon cancer (CAC). *Sophora japonica* is a medicinal and food plant commonly used to treat hemorrhoids, bleeding, and inflammation, symptoms that coincide with those of patients with CAC. However, studies on using *Sophora japonica* to treat CAC are scarce. Therefore, this study aimed to investigate the anti-inflammatory and antitumor effects of *Sophora japonica* extract (SJE) using dextran sodium sulfate (DSS)-induced UC and azoxymethane (AOM)/DSS-induced CAC models. Furthermore, we employed ultraperformance liquid chromatography–quadrupole time-of-flight–tandem mass spectrometry (UPLC–QTOF–MS/MS) technology to explore the metabolomics mechanism through which SJE inhibited the progression of UC to CAC. The results demonstrated that SJE significantly inhibited UC and CAC and alleviated symptoms such as bloody stools, colon shortening, inflammation, and intestinal tissue damage in model mice. Further, 57 differential metabolites were identified by UPLC–QTOF–MS/MS, which were composed mainly of lipids (fatty acids, glycerophospholipids, sterol lipids, pregnenolone lipids, etc.) and peptides (amino acids). Kyoto Encyclopedia of Genes and Genomes (KEGG) enrichment analysis suggested that SJE might inhibit the progression of UC to CAC by regulating lipid metabolic pathways such as arachidonic acid metabolism, primary bile acid biosynthesis, and linoleic acid metabolism. This study, for the first time, substantiated the inhibitory effect of SJE on CAC. Employing metabolomics techniques, the research delved into the potential pathways through which SJE may exert its inhibitory effects on CAC by suppressing the progression of UC. These findings contribute scientific evidence to the application of *Sophora japonica* in functional foods and the development of natural drugs for the prevention and treatment of UC and CAC.

1. Introduction

Ulcerative colitis (UC) is a chronic nonspecific inflammatory bowel disease affecting the colonic mucosa. It has been classified as one of the difficult-to-treat illnesses by the World Health Organization due to its long course, persistent symptoms, and high risk of recurrence [1]. Unfortunately, the symptoms of UC during its development are often overlooked, and prolonged UC aggravates the likelihood of numerous complications. One of the most serious and life-threatening complications is colorectal cancer (CRC), and colitis-associated colon cancer (CAC) is the primary cause of colon resection and mortality in this population [2, 3]. Epidemiological studies have reported that patients with UC are two to eight times more likely to develop CAC [4, 5]. Increasing evidence suggests that controlling chronic inflammation and mucosal damage is crucial for developing the disease, and adopting a maintenance therapy approach for chronic UC may serve as a vital strategy for reducing the risk of CAC in patients with UC [6].

According to the clinical manifestations of abdominal pain, diarrhea, and purulent bloody stool, UC belongs to "diarrhea,"

"dysentery," "intestinal wind," and "hematochezia" in traditional medicine, presenting the pathological changes in terms of dampness and heat in the intestines and the imbalance of qi and blood, with dampness and heat being the main pathological factors, and dampness and heat in the large intestine are the core symptoms [7–9]. *Sophora japonica* belongs to the large intestine meridian; has efficacy in terms of cooling blood, stopping bleeding, and clearing the liver and cathartic fire and is used to treat blood in stool, hemorrhoidal blood, bloody dysentery, and so forth. Therefore, it is commonly used for treating UC to improve intestinal bleeding and inflammation [10, 11].

Sophora japonica, as a plant with the homology of medicine and food, is often made into dishes and tea in Asia (especially in China) [10, 12]. Modern pharmacological research has shown that *Sophora japonica* has anti-inflammatory [12, 13], hypoglycemic action [14], antimicrobial [15], antioxidant [16], and treatment effects on hyperuricemia [17], among others. *Sophora japonica* is rich in chemical components, mainly including flavonoids, saponins, alkaloids, and polysaccharides [10, 17]. By reviewing the literature [10, 18–21] and analyzing the components of *Sophora japonica* extract (SJE) in the early stage of the study, we found multiple antitumor-active ingredients in *Sophora japonica*, such as rutin, genistein, sophoridine, matrine, and quercetin. Combined with the symptoms of colorectal cancer-related rectal bleeding, we speculated that *Sophora japonica* might have a certain preventive and protective effect on inflammation-related cancer through its anti-inflammatory and hemostatic effects, but relevant studies are scarce. Therefore, we established UC and CAC animal models and first demonstrated the inhibitory effect of SJE on CAC. We used metabolomics to investigate the metabolic disturbances induced by the UC and CAC models and to explore the potential mechanisms underlying the inhibition of chronic colitis and related cancers by SJE. We aimed to offer a scientific foundation for developing and using SJE as a medicinal agent for preventing and treating CAC.

2. Materials and Methods

2.1. Animals. Male BALB/c mice weighing 20 ± 2 g and in good health were procured from Liaoning Changsheng Biotechnology Co., Ltd., and maintained under standard laboratory conditions at a temperature of 25°C ± 2°C, relative humidity of 55% ± 5%, and natural light/dark cycle. The mice were acclimatized for 1 week and had free access to food and water prior to experimentation. The certificate of conformity number for the experimental animals was SCXK (Liao) 2020-0001.

2.2. Preparation of SJE. Appropriate amounts of *Sophora japonica* were pulverized and mixed with 10 times the amount of 50% ethanol. Ultrasonic extraction (at a power of 200 W and a frequency of 40 kHz) was performed for 1 h. The resulting extract was filtered, and the ethanol was recovered until the filtrate was devoid of any alcohol odor. The extract was then diluted with water to the desired concentration for administration, mixed thoroughly, and stored at 4°C until use.

2.3. Experimental Design for UC and CAC. For the UC experiment, the mice were randomly classified into six groups: a control (CON) group, a model (DSS) group, a low-dose SJE (DSS + LSJE, 3.9 g/kg) group, a medium-dose SJE (DSS + MSJE, 11.7 g/kg) group, a high-dose SJE (DSS + HSJE, 35.1 g/kg) group, and mesalazine enteric-coated tablets positive control (DSS + MES, 0.078 g/kg) group (batch number 210112, produced by Khuh Pharm Co., Ltd., Jiamusi, China), with eight mice in each group. The dosages were based on human equivalent doses. Except for the CON group, the mice in all other groups were given 2.5% DSS (batch number: M0510B; Meilunbio Co., Ltd., China) in their drinking water for seven consecutive days to induce colitis, followed by 14 days of drinking regular water. This 21-day cycle of DSS treatment and free access to water was repeated three times. Meanwhile, the oral gavage of the test substances began after the first cycle and continued until the end of the third cycle. Body weight and fecal occult blood were monitored weekly during the experiment.

For the CAC experiment, male BALB/c mice weighing 20 ± 2 g were randomly divided into the control (CON) group, the model (AOM + DSS) group, the low-dose SJE (AOM + DSS + LSJE, 3.9 g/kg) group, the medium-dose SJE (AOM + DSS + MSJE, 11.7 g/kg) group, the high-dose SJE (AOM + DSS + HSJE, 35.1 g/kg) group, and the capecitabine tablet–treated positive control (AOM + DSS + CAPE, 0.13 g/kg) group (batch number: 1B0213DE3; Qilu Pharmaceutical Co., Ltd.), with eight mice per group. Except for the CON group, the mice in the model group were intraperitoneally injected with azoxymethane (AOM) at a dose of 10 mg/kg (purity 95%, batch number: A1908142; Aladdin) and given 2.5% DSS in drinking water for 7 days after 1 week, followed by free access to distilled water for 14 days. The aforementioned 21-day cycle of DSS and distilled water was repeated three times. Meanwhile, the mice were orally administered the test substances starting from the end of the first cycle until the end of the third cycle. Body weight was monitored weekly throughout the experiment.

2.4. Collection of Tissues and Blood Samples. At the end of the experiment, the mice were fasted for 24 h prior to collecting blood and tissue samples. Blood was allowed to clot for 15 min, followed by centrifugation at 2500 rpm for 10 min to obtain serum, which was then stored at −80°C until further use. The colon length was measured, and the tissue was washed and weighed. A 2-cm segment of the distal colon near the anus was cut and fixed in 4% paraformaldehyde for pathological sectioning. The spleen and thymus were collected and weighed for immunological analysis.

2.5. Histological Analysis. The colon tissues were processed for pathological analysis. Specifically, they were fixed in 4% paraformaldehyde, embedded in paraffin, and sectioned into 5-μm-thick slices. The evaluation of the pathological status of UC (see Table S1 for scoring criteria) and CRC (see Table S2 for scoring criteria) was conducted through hematoxylin and eosin (H&E) staining, which was performed

in a blinded manner by trained personnel. The images were captured using a bright-field microscope (Eclipse Ci-L; Nikon), scanning software (3DHISTECH, CaseViewer2.4), and a panoramic slide scanner (3DHISTECH, PANNORAMIC DESK/MIDI/250/1000), and the analysis was performed by Wuhan Cever Biotechnology Co., Ltd.

2.6. Inflammatory Cytokine Detection. The enzyme-linked immunosorbent assay (ELISA) kits from Shanghai Kexing Biotech Co., Ltd., were used to measure the levels of tumor necrosis factor (TNF)-α (lot number: 21071230N), interleukin (IL)-6 (lot number: 21071233N), and IL-1β (lot number: 20171235N) in serum following the manufacturer's protocols.

2.7. Serum Metabolomics Analysis. The serum samples (100 μL) were prepared by adding 300 μL of 0.1% formic acid–methanol and vortexing for 3 min. The mixture was then sonicated for 5 min and left overnight at 4°C. The next day, the mixture was centrifuged at 12,000 rpm for 10 min, and the supernatant (100 μL) was transferred to a new tube and dried using vacuum centrifugation. The residue was dissolved in 50 μL of 70% methanol and vortexed for 3 min before sonication for 5 min. After centrifugation at 12,000 rpm for 10 min, the supernatant was collected for UPLC-QTOF-MS analysis. A quality control (QC) sample was prepared by pooling 10 μL of the supernatant from each sample.

The UPLC-QTOF-MS system (Agilent 1290 UPLC coupled with an Agilent G6550 Q-TOF-MS) was used for separation using a poroshell SB-C18 120 chromatographic column ($100 \times 2.1\ mm^2$, 2.7 μm). The positive ion-mode mobile phase consisted of 0.1% formic acid water (A) and methanol (B), whereas the negative ion mode mobile phase consisted of 0.1% formic acid water (A) and acetonitrile (B). The optimized gradient for positive ion mode was 0–6 min, 95%–35% A; 6–13 min, 35%–20% A; 13–27 min, 13%–8%A; and 27–30 min, 8%–0% A. The optimized gradient for negative ion mode was 0–30 min, 95%–0% A. The flow rate was set at 0.4 mL/min, and the column temperature was maintained at 30°C. Electro spray ionization (ESI) was used to collect data in both positive and negative ion modes. The mass range was 100–1000 m/z, and the collision voltage was set at 125 V.

The mass spectrometry data were processed using Agilent MassHunter Profinder 08.00 software, which involved peak detection, peak alignment, and normalization. Compound data files were extracted, and data with an RSD >30% in the QC sample were removed. Differential metabolites were screened using MetaboAnalyst 5.0 software with partial least squares discriminant analysis (PLS-DA) and orthogonal PLS-DA (OPLS-DA) based on Variable Importance in Projection (VIP) > 1, $P < 0.05$, FC > 1.5, or FC < 0.67. Short time-series expression miner (STEM) was used to identify metabolites that reverted to the CON group. Furthermore, the fragmentation patterns of the metabolites were compared with databases such as Metlin and The Human Metabolome Database (HMDB), as well as standard compounds, for identification. Pathway enrichment analysis and visualization were conducted using MetaboAnalyst 5.0.

2.8. Statistical Analysis. The data were expressed as mean ± standard deviation (SD). Statistical analysis and data visualization were performed using GraphPad Prism 8.0. The unpaired-samples Student's t-test was employed to compare the differences between the two groups, while one-way analysis of variance was used for multiple group comparisons. The threshold for statistical significance was set at $P < 0.05$.

3. Results

3.1. SJE Suppressed DSS-Induced UC Development. The body weight and occult blood of mice were monitored and recorded weekly during the experiment to evaluate the protective effects of SJE on UC. No abnormal symptoms were observed in the CON group throughout the experiment. The mice in the DSS group showed fluctuations in body weight from the third week and exhibited symptoms such as diarrhea and positive occult blood during the DSS intervention period (Figures 1(a) and 1(b)). The aforementioned symptoms in mice improved in the SJE groups compared with the DSS group. The colon of mice in the DSS group was significantly shortened, the tissue was thickened, the elasticity reduced, and brittleness increased on hand touch (Figures 1(c) and 1(d)). Additionally, the colon weight-to-length ratio increased (Figure 1(e)), and the spleen and thymus indexes also increased (Figures 1(f) and 1(g)). However, these symptoms were significantly alleviated in the SJE groups. ELISA results showed that SJE could regulate the significant increase in the serum levels of inflammatory factors TNF-α, IL-6, and IL-1β induced by DSS intervention (Figures 1(h)–1(j)). The histological examination showed that DSS intervention caused pathological changes in the colon tissue, including mucosal layer necrosis, reduced number of intestinal glands, increased connective tissue hyperplasia, and moderate infiltration of lymphocytes and neutrophils. In some samples, ulcers, epithelial cell shedding, and infiltration of inflammatory cells into the submucosal layer were also observed. Treatment with different concentrations of SJE significantly reduced colon tissue damage (Figures 1(k) and 1(l)).

3.2. SJE Inhibited AOM/DSS-Induced CAC Development. We monitored and recorded the body weight and fecal blood of mice every week during the experiment to evaluate the protective effect of SJE on CAC. The AOM + DSS model mice exhibited significant diarrhea, bloody stools, and even prolapse of the anus in the ninth week (Figures 2(a) and 2(b)). Colon tissue examination of the AOM + DSS group mice showed that the colon length was significantly shortened and edema was apparent compared with the CON group, and multiple adenomas and bleeding sites in the colon tissue were observed. However, the colon length of mice in each concentration

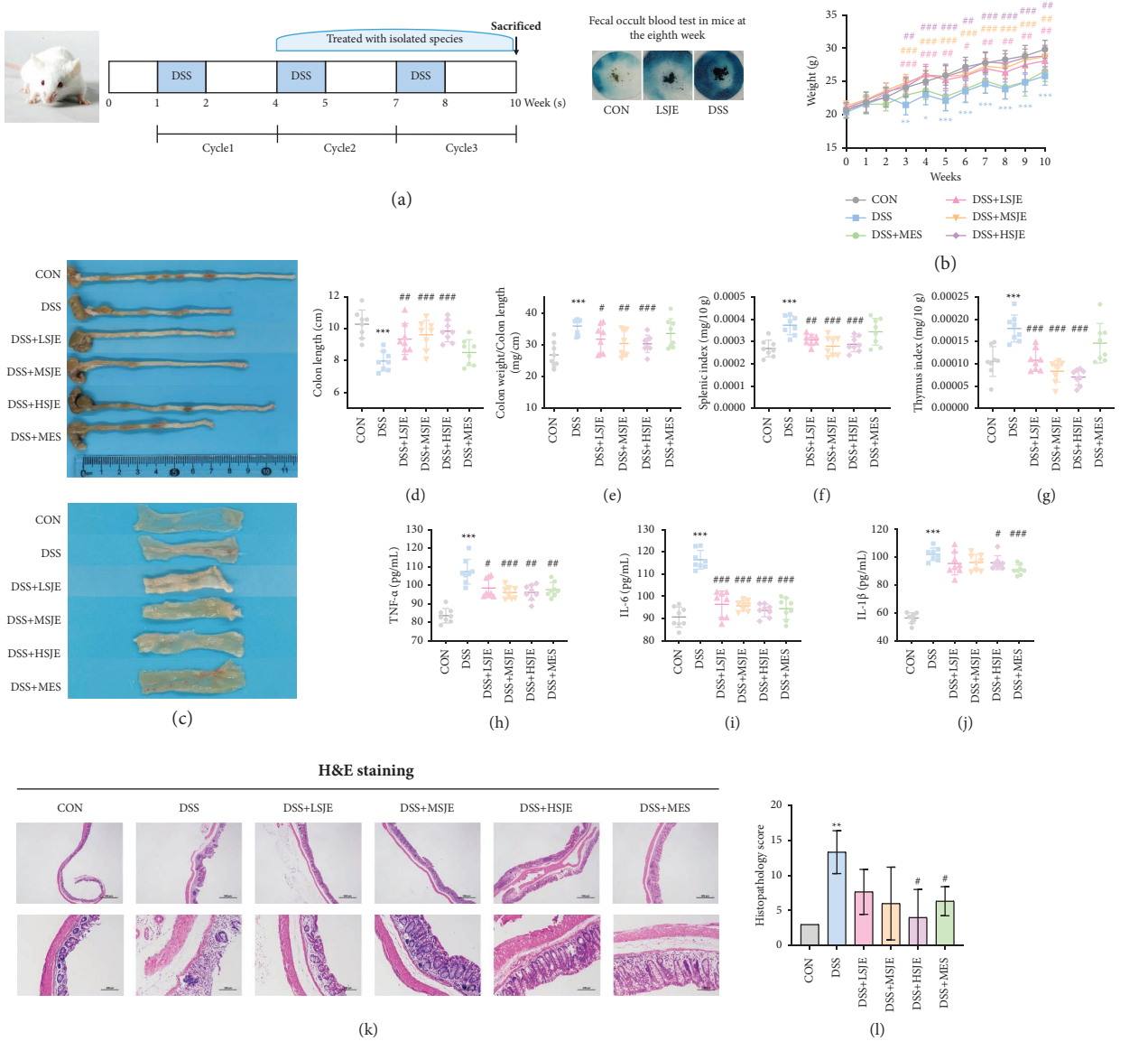

Figure 1: SJE inhibited DSS-induced UC development. (a) Experimental scheme and sample intervention of the UC mouse model. (b) Average weekly body weight of each group of mice during the experiment. (c) Photographs of colon tissues of mice at the experimental endpoint. (d) Changes in colon length. (e) Ratio of colon weight to length. (f) Spleen index. (g) Thymus index. (h) Serum TNF-α level in mice. (i) Serum IL-6 level in mice. (j) Serum IL-1β level in mice. (k) H&E staining (40x and 200x magnification) showing pathological changes in intestinal tissues. (l) Analysis of tissue pathological scores for each group. The data are presented as mean ± SD. $^{*}P < 0.05$, $^{**}P < 0.01$, $^{***}P < 0.001$ compared with the CON group; $^{\#}P < 0.05$, $^{\#\#}P < 0.01$, $^{\#\#\#}P < 0.001$ compared with the DSS group.

of the SJE group was significantly larger than that of the AOM + DSS group, and no obvious edema or bleeding phenomenon was noted (Figures 2(c) and 2(d)). At the same time, the colon weight-to-length ratio in the AOM + DSS group mice increased (Figure 2(e)), and the spleen and thymus indexes also increased (Figures 2(f) and 2(g)). The various concentrations of SJE alleviated the aforementioned symptoms. The CON group did not show obvious adenomas in the colon, while the adenoma formation rate in the AOM + DSS group was 100%, with an average number of colon adenomas per mouse of 19 ± 5.13. The high-dose SJE group had significantly fewer adenomas with smaller diameters, while the low- and medium-dose groups had significantly better adenoma numbers than the AOM + DSS group, although the diameters were not significantly reduced (Figures 2(h) and 2(i)). Additionally, the histological examination showed that SJE treatment significantly reduced the characteristic pathological symptoms caused by AOM + DSS, including large areas of tissue carcinogenesis, glandular hyperplasia, increased nuclear–cytoplasmic ratio, nuclear division, tumor cell necrosis, lymphocyte infiltration, connective tissue proliferation, and epithelial cell shedding (Figures 2(j) and 2(k)). These results suggested that SJE had a good preventive and inhibitory effect on tumor occurrence in the mouse CAC model.

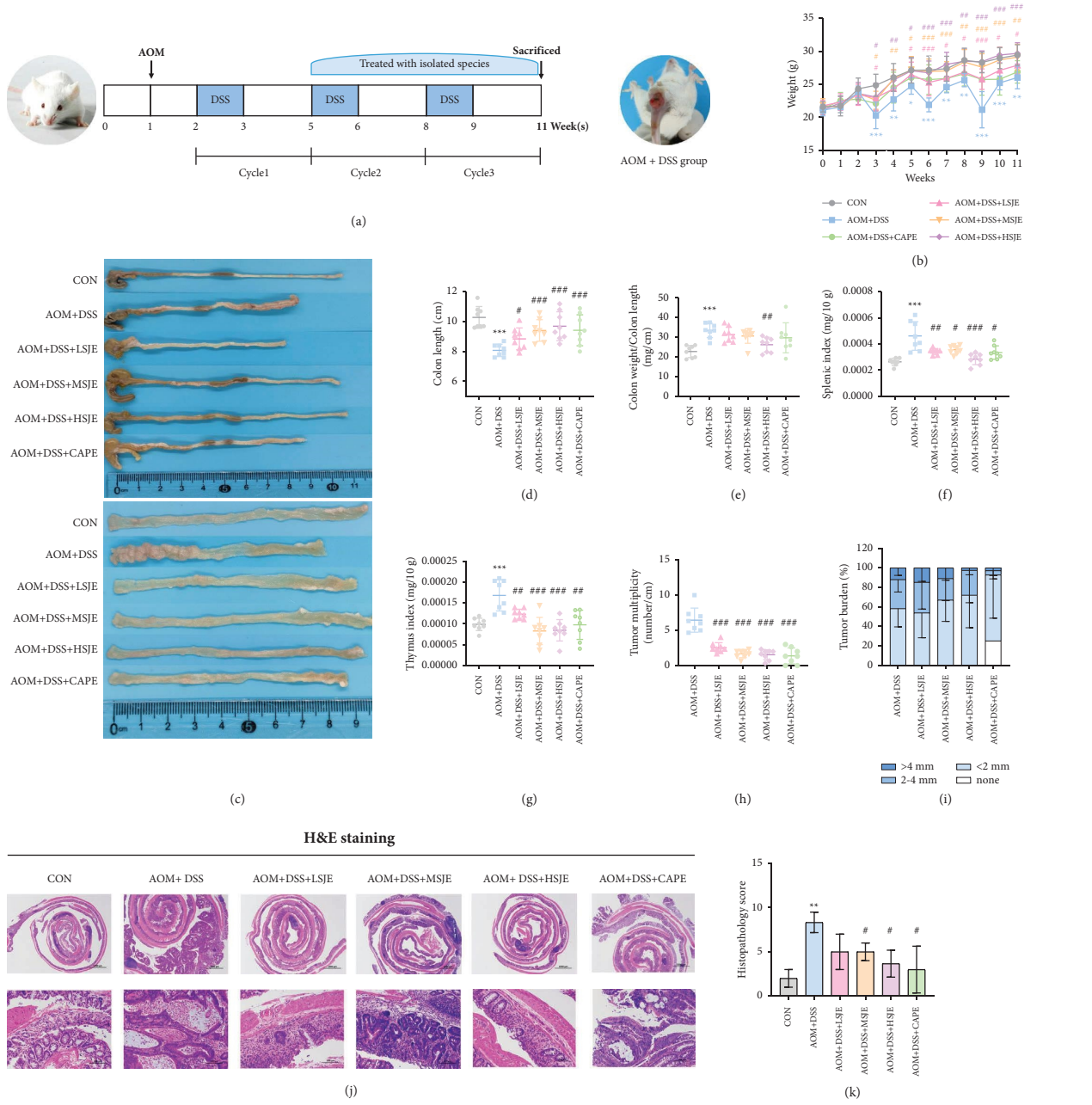

Figure 2: SJE inhibited AOM/DSS-induced CAC development. (a) Experimental design and sample intervention of CAC mouse model. (b) Average weekly body weight of each group during the experiment (g). (c) Representative images of colon tissues at the experimental endpoint. (d) Changes in colon length. (e) Ratio of colon weight to length. (f) Tumor multiplicity. (g) Spleen index. (h) Thymus index. (i) Tumor burden at the experimental endpoint. (j) H&E staining (20x and 200x magnification) displaying pathological changes in tumor tissues. (k) Histopathological score analysis for each group. The data are presented as mean ± SD. $^{*}P < 0.05$, $^{**}P < 0.01$, $^{***}P < 0.001$, compared with the CON group; $^{\#}P < 0.05$, $^{\#\#}P < 0.01$, $^{\#\#\#}P < 0.001$, compared with the DSS group.

3.3. QC of Metabolomics Analysis. We analyzed the serum metabolic profiles of UC and CAC experimental groups based on untargeted metabolomics analysis, and the representative total ion chromatograms (TICs) obtained from the serum samples are shown in Figure 3. We used QC samples in both positive and negative ion modes to evaluate the stability and reliability of the experimental method. The PLS-DA model was used to evaluate the samples. The QC samples, CON group, model group, and treatment group were significantly clustered, and every experimental group could be clearly distinguished. This indicated that the experimental method was stable and the data quality was high (Figure S1). After RSD screening of the QC samples, 1259 (negative ion mode) and 4539 (positive ion mode) characteristic metabolites were left in the UC experimental serum samples, and 1776 (negative ion mode) and 4089 (positive ion mode) characteristic metabolites were left in the CAC experimental serum samples. The metabolites identified in both positive and negative ion modes were combined for further analysis.

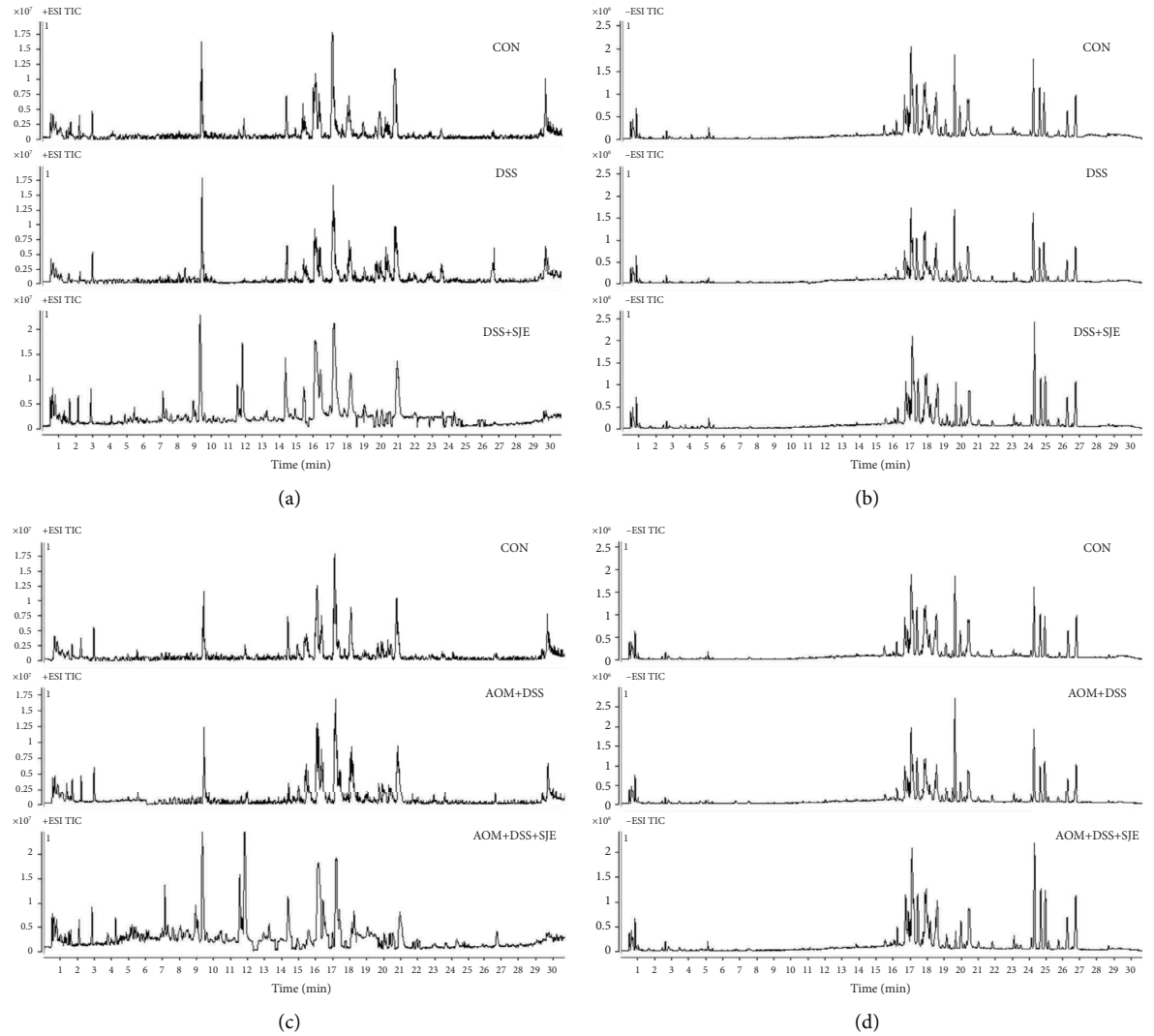

Figure 3: Representative TICs for each group of samples in positive ion mode (a and c) and negative ion mode (b and d).

3.4. Metabolic Profiling of UC and CAC Mouse Serum. We compared the serum metabolomes of the CON and DSS groups, and CON and AOM + DSS groups in UC and CAC experiments, respectively, to observe the metabolic changes induced by modeling. OPLS-DA models showed a clear separation of the model groups from the CON groups, indicating significant metabolic disturbances caused by DSS-induced UC and AOM/DSS-induced CAC (Figures 4(a) and 4(d)). $R^2Y = 0.925$, $Q^2 = 0.729$ for the UC experiment and $R^2Y = 0.981$, $Q^2 = 0.834$ for the CAC experiment (Figures 4(b) and 4(e)), indicating that the models had good fitting and predictive abilities and could be used for differential marker screening. Based on VIP >1, $P < 0.05$, FC > 1.5, or FC < 0.67 as screening criterion, we identified 281 and 240 significantly different metabolites for UC and CAC experiments, respectively, by matching the METLIN and HMDB databases (Figures 4(c) and 4(f)). We submitted 281 and 240 significantly different metabolites in serum to MetaboAnalyst 5.0 for the Kyoto Encyclopedia of Genes and Genomes (KEGG) pathway enrichment analysis to explore the abnormal changes in the metabolic pathways of UC and CAC. The top 20 enriched abnormal metabolic pathways in UC and CAC models mainly included lipid metabolism, amino acid metabolism, cofactors and vitamin metabolism, and nucleotide metabolism, among others (Figures 4(g) and 4(h)). Specifically, the biosynthesis of phenylalanine, tyrosine, and tryptophan; purine metabolism, arachidonic acid (AA) metabolism, phenylalanine metabolism, taurine and hypotaurine metabolism, and linoleic acid (LA) metabolism; and primary bile acid (BA) biosynthesis were significantly enriched in UC and might play important roles in UC development. These pathways were also significantly enriched in CAC, suggesting that they might play important roles in the progression from UC to CAC. Further, glycerophospholipid metabolism, ubiquinone and other terpenoid-quinone biosynthesis, and alpha-linolenic acid metabolism might also play roles in CAC development.

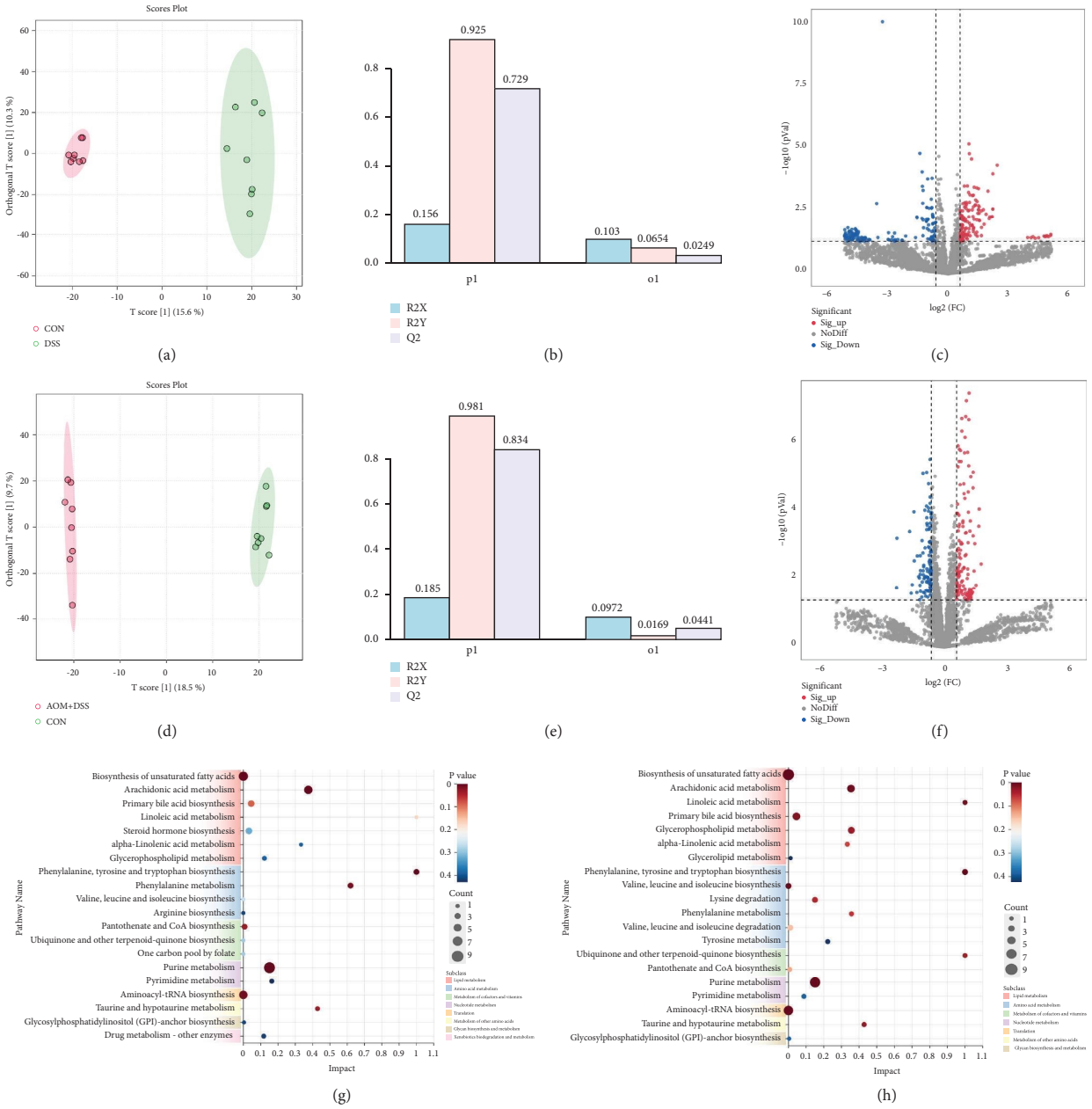

Figure 4: Metabolomic analysis of serum in mice with UC and CAC. (a) OPLS-DA was used to analyze the metabolites in serum samples of mice with UC in the CON and DSS groups. (b)R^2Y and Q^2 values were used to evaluate the predictive ability of the OPLS-DA model in UC experiments. (c) Volcano plot of differential metabolites between the CON and DSS groups in UC experiments. (d) OPLS-DA was used to analyze the metabolites in serum samples of mice with CAC in the CON and AOM + DSS groups. (e)R^2Y and Q^2 values were used to evaluate the predictive ability of the OPLS-DA model in CAC experiments. (f) Volcano plot of differential metabolites between the CON and AOM + DSS groups in CAC experiments. (g) Bubble plots of metabolic pathways enriched by abnormal metabolites in mice with UC. (h) Bubble plots of metabolic pathways enriched by abnormal metabolites in mice with CAC. The vertical axis represents KEGG pathway names, the horizontal axis represents weight values based on topological analysis, and the color of the bubble represents the P value. The size of the bubble represents the number of metabolites. Different colors of the subclass are used to distinguish different types of metabolic pathways.

3.5. Effects of SJE on Metabolic Profiles in Mice with UC and CAC. The serum metabolic profiles of mice in the DSS and DSS + SJE groups and the AOM + DSS and AOM + DSS + SJE groups were compared to investigate the regulatory effects of SJE on metabolic disorders in the models. OPLS-DA models showed that the model groups of UC and CAC were significantly separated from the SJE group, indicating that SJE could regulate the metabolic disorder induced by UC and CAC (Figures 5(a) and 5(b)). STEM analysis was conducted on CON, DSS, and DSS + SJE groups, as well as CON, AOM + DSS, and AOM + DSS + SJE groups to identify the differential metabolites regulated by SJE. Metabolites with

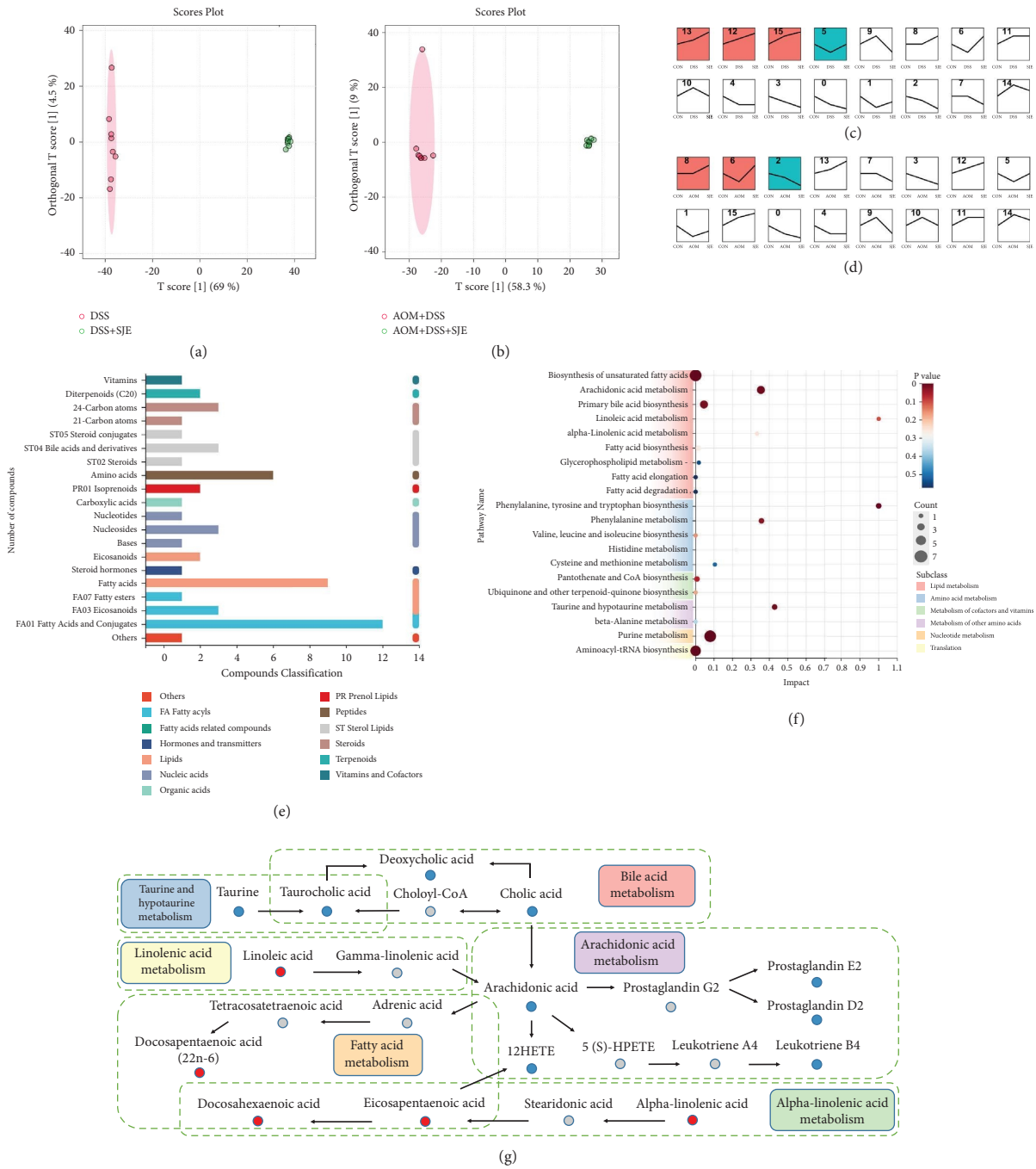

Figure 5: Effects of SJE on metabolic expression profiles in mice with UC and CAC. (a) OPLS-DA analysis of metabolites between the SJE and DSS groups in the UC experiment. (b) OPLS-DA analysis of metabolites between the SJE and AOM + DSS groups in the CAC experiment. (c) STEM analysis was used to screen metabolites that were restored to the CON group in the UC experiment. (d) STEM analysis was used to screen metabolites that were restored to the CON group in the CAC experiment. (e) Classification of common differential metabolites (the vertical axis represents the type of metabolite, and the horizontal axis represents the number of metabolites). (f) Bubble chart showing the enriched pathways modulated by SJE intervention (the vertical axis represents KEGG pathway names, the horizontal axis represents weight values based on topological analysis, the bubble color represents *P* values, and the bubble size represents the number of metabolites; subclass colors are used to distinguish between different metabolic pathway categories). (g) Metabolic pathways influenced by SJE intervention.

a trend of returning to the CON group were identified in profiles 1, 5, 6, 9, 10, and 14 (Figures 5(c) and 5(d)), and the fraction of them that were identical to the significantly different metabolites of UC and CAC might be essential for SJE to inhibit the development of UC and the progression of UC to CAC. UPLC–QTOF–MS/MS was then used to identify the fragments of the aforementioned metabolites and compared them with standard substances and databases, identifying 57

differential metabolites (Table 1). These metabolites were mainly concentrated in lipids (fatty acids, glycerophospholipids, sterol lipids, pregnenolone, ketosterol lipids, etc.) and peptides (amino acids) (Figure 5(e)). Metabolic pathways were mainly enriched in lipid metabolism pathways such as AA metabolism, primary BA biosynthesis, and LA metabolism, as well as amino acid metabolism pathways (Figure 5(f)). Therefore, we established a metabolic network based on lipid metabolism pathways to reveal the regulatory mechanisms of these metabolites on UC and CAC and their interactions (Figure 5(g)). Red metabolites represented upregulated metabolites after SJE intervention, whereas blue metabolites represented downregulated metabolites. These metabolites might be critical pathways for the inhibitory effects of SJE on the UC-to-CAC transition.

4. Discussion

It has been confirmed that chronic inflammation contributes to the development and progression of CAC, and cytokines produced by inflammatory and intestinal epithelial cells are among the mechanisms driving carcinogenesis. Cytokine stimulation leads to complex interactions between intestinal epithelial cells and immune system cells in the gut, disrupting tolerance to the gut microbiota and disturbing the balance between pro-inflammatory and anti-inflammatory signals, resulting in changes in cellular behavior and the onset of cancer [3, 22]. Therefore, a treatment strategy that can effectively control chronic inflammation may be an effective form of prevention and treatment for CAC.

DSS-induced mice with colitis and AOM/DSS-induced mice with colon cancer exhibit symptoms similar to those of patients with UC and CAC, respectively, including weight loss, diarrhea, rectal bleeding, colonic shortening, inflammatory responses, and intestinal tissue damage [23]. Thus, DSS and AOM/DSS are widely used for establishing mouse colitis and colon cancer models. Traditional Chinese medicine holds that *Sophora japonica* can cool the blood and stop bleeding. In pharmacological experiments, it can be seen that SJE has good controlling effects on occult blood in UC and bleeding symptoms in CAC, and it alleviates the pathological symptoms such as weight loss, diarrhea, colon shortening, and inflammation caused by UC and CAC models to varying degrees. Moreover, SJE significantly controls the number of colon adenomas and tissue carcinogenesis caused by CAC, indicating that SJE has protective effects on CAC.

In the metabolomic analysis of UC and CAC, lipid metabolism, amino acid metabolism, nucleotide metabolism, and translation showed significant metabolic disorders. SJE effectively regulated the aforementioned metabolic disorders. We further characterized the metabolites by UPLC-QTOF-MS/MS to improve the accuracy. We found that 60% of the 57 identified differential metabolites were lipids, which were significantly enriched in lipid metabolism pathways such as AA metabolism, LA metabolism, BA metabolism, and so forth. Therefore, we speculated that regulating lipid metabolism by SJE might be the key pathway to inhibit UC and CAC. Significant perturbations in metabolic pathways related to fatty acid biosynthesis, detectable in serum several years prior to diagnosis, have been detected in patients with UC, and perturbations in the metabolism of serum lipids and sphingolipids have been found in newly diagnosed patients with UC [24]. Andrew Gold et al. analyzed 37 studies characterizing the metabolomics of CRC reported between January 2012 and July 2021 and found that a large number of metabolites were differentially regulated in patients with CRC, with dysregulation of metabolic biomarkers such as certain amino acids, fatty acids, and lysophosphatidylcholines (LPCs) being particularly pronounced [25]. This was in line with our findings. The abnormal metabolism of lipids is an essential phenotype of cancer cells, including CAC [26, 27]. Cancer cells activate aberrant lipid metabolism by increasing the uptake of exogenous lipids or endogenous lipid generation to meet the needs of continuous proliferation, invasion, and metastasis, as well as to obtain energy and respond to the impact of the tumor microenvironment [28]. Additionally, the cross-regulation between lipid metabolism and pro-cancer signaling pathways also promotes the growth and metastasis of cancer cells. The metabolomic analysis of UC and CAC showed that lipid metabolism, represented by AA metabolism, LA metabolism, and primary BA biosynthesis, showed significant disorders. Previous studies also found that these metabolic pathways played substantial roles in developing inflammation and cancer.

AA is metabolized by the cyclooxygenase (COX) pathway to produce prostaglandins (PGs), which act as critical inflammatory mediators in the inflammatory process, such as vasodilation, increased permeability of capillary walls, and enhanced pain and tissue swelling effects of histamine and kinins [29, 30]. Inhibiting the generation and function of PGs can effectively inhibit inflammation. Additionally, AA is metabolized by the lipoxygenase pathway to produce many hydroperoxy fatty acids, including 5-hydroxyeicosatetraenoic acid (5-HPETE) and 12-hydroxyeicosatetraenoic acid (12-HPETE), which indirectly activate COX pathway metabolism. 5-HPETE further converts into leukotrienes, which can enhance vascular permeability, leading to edema at the site of inflammation [30]. 12-HPETE is catabolized to 12-hydroxyeicosatetraenoic acid (12-HETE), which is involved in increased inflammation and platelet activation [31]. Several preclinical *in vitro* studies, including on nonsteroidal anti-inflammatory drugs such as aspirin, have shown that the inhibition of COX-2 can suppress the progression of adenomas to adenocarcinomas [32]. Epidemiological and clinical trial studies also support the effectiveness of this class of anti-inflammatory drugs in reducing the risk of CRC. Therefore, it is feasible to control inflammation and cancer development by regulating the AA metabolic pathway. Our study found that SJE alleviated inflammation symptoms and intestinal tissue edema in the UC and CAC models. SJE had a regulatory effect on AA, prostaglandin E2, leukotriene B4, and 12-HETE, suggesting that SJE might inhibit the development of UC to CAC by regulating AA metabolism.

Table 1: Endogenous differential metabolites identified in serum.

No	ESI mode	Metabolites	Formula	Molecular weight	RT (min)	*m/z*	Control vs model trend
1*	–	Taurine	$C_2H_7NO_3S$	125.1470	0.611	124.0081	Down
2[a]	–	Uric acid	$C_5H_4N_4O_3$	168.1103	0.668	167.0208	Down
3*	–	L-Histidine	$C_6H_9N_3O_2$	155.1546	0.695	154.0614	Up
4*	–	L-Valine	$C_5H_{11}NO_2$	117.1463	0.752	116.0724	Up
5*	–	L-Tyrosine	$C_9H_{11}NO_3$	181.1885	1.091	180.0676	Up
6[a]	–	Deoxyuridine	$C_9H_{12}N_2O_5$	228.2020	1.728	227.0682	Up
7*	–	Inosine	$C_{10}H_{12}N_4O_5$	268.2261	1.937	267.0720	Up
8[a]	–	Guanosine	$C_{10}H_{13}N_5O_5$	283.2407	1.956	282.0848	Up
9*	–	Pantothenic acid	$C_9H_{17}NO_5$	219.2350	2.079	218.1030	Up
10[a]	–	2-Methylbutanoic acid	$C_5H_{10}O_2$	102.1317	2.193	101.0605	Up
11[a]	–	D-Phenylalanine	$C_9H_{11}NO_2$	165.1891	2.276	164.0714	Up
12[a]	–	Adenine	$C_5H_5N_5$	135.1267	3.434	134.0472	Down
13[a]	–	DL-Tryptophan	$C_{11}H_{12}N_2O_2$	204.2252	3.461	203.0813	Up
14[a]	–	Indoxyl sulfate	$C_8H_7NO_4S$	213.2100	6.905	212.0023	Up
15[a]	–	p-Cresol sulfate	$C_7H_8O_4S$	188.2010	10.179	187.0054	Up
16*	–	Prostaglandin E2	$C_{20}H_{32}O_5$	352.4651	13.526	351.2175	Down
17[a]	–	Prostaglandin D2	$C_{20}H_{32}O_5$	352.4651	15.841	351.2176	Down
18[a]	–	Leukotriene B4	$C_{20}H_{32}O_4$	336.4657	17.687	335.2230	Down
19[a]	–	Taurocholic acid	$C_{26}H_{45}NO_7S$	515.7030	18.042	514.2848	Down
20[a]	–	Deoxycholic acid	$C_{24}H_{40}O_4$	392.5720	21.103	391.2847	Down
21[a]	–	12-Hydroxyeicosatetraenoic acid	$C_{20}H_{32}O_3$	320.4663	21.300	319.2279	Down
22[a]	–	9,12-Octadecadiynoic acid	$C_{18}H_{28}O_2$	276.4200	22.345	275.2002	Up
23[a]	–	7Z,10Z-hexadecadienoic acid	$C_{16}H_{28}O_2$	252.3923	22.598	251.2001	Up
24[a]	–	Myristic acid	$C_{14}H_{28}O_2$	228.3709	23.066	227.2009	Up
25[a]	–	Alpha-linolenic acid	$C_{18}H_{30}O_2$	278.4296	23.163	277.2157	Up
26[a]	–	Methenolone	$C_{20}H_{30}O_2$	302.4510	23.179	301.2154	Up
27[a]	–	Palmitoleic acid	$C_{16}H_{30}O_2$	254.4082	23.388	253.2165	Up
28[a]	–	Pentadecanoic acid	$C_{15}H_{30}O_2$	242.3975	23.474	241.2171	Down
29*	–	Arachidonic acid	$C_{20}H_{32}O_2$	304.4669	23.744	303.2311	Down
30[a]	–	Linoleic acid	$C_{18}H_{32}O_2$	280.4455	23.784	279.2313	Up
31[a]	–	Docosahexaenoic acid	$C_{22}H_{32}O_2$	328.4883	23.800	327.2308	Up
32[a]	–	Docosapentaenoic acid (22*n*-6)	$C_{22}H_{34}O_2$	330.5042	24.082	329.2491	Up
33[a]	–	Palmitic acid	$C_{16}H_{32}O_2$	256.4241	24.122	255.2319	Up
34[a]	–	Adrenic acid	$C_{22}H_{36}O_2$	332.5200	24.703	331.2628	Up
35*	–	Stearic acid	$C_{18}H_{36}O_2$	284.4772	25.364	283.2653	Up
36[a]	+	5-amino valeric acid betaine	$C_8H_{17}NO_2$	159.2290	0.702	160.1326	Up
37[a]	+	3′-AMP	$C_{10}H_{14}N_5O_7P$	347.2212	0.868	348.0692	Down
38*	+	L-Methionine	$C_5H_{11}NO_2S$	149.2110	0.928	150.0578	Up
39[a]	+	Adenosine	$C_{10}H_{13}N_5O_4$	267.2413	1.178	268.1013	Up
40[a]	+	Xanthine	$C_5H_4N_4O_2$	152.1109	1.285	153.0396	Up
41*	+	Hypoxanthine	$C_5H_4N_4O$	136.1115	1.961	137.0463	Up
42*	+	L-Phenylalanine	$C_9H_{11}NO_2$	165.1891	2.531	166.0859	Up
43[a]	+	Pyrogallol-2-O-glucuronide	$C_{12}H_{14}O_9$	302.2342	2.741	325.0526	Up
44[a]	+	Butyrylcarnitine	$C_{11}H_{21}NO_4$	231.2920	2.797	232.1516	Down
45[a]	+	L-Tryptophan	$C_{11}H_{12}N_2O_2$	204.2252	4.113	205.0967	Up
46[a]	+	Corticosterone	$C_{21}H_{30}O_4$	346.4605	11.253	347.2198	Up
47[a]	+	Beta-muricholic acid	$C_{24}H_{40}O_5$	408.5790	13.952	431.2745	Down
48[a]	+	Tetradecanoylcarnitine	$C_{21}H_{42}NO_4$	372.5690	14.918	372.3095	Up
49*	+	Cholic acid	$C_{24}H_{40}O_5$	408.5714	15.498	431.2745	Down
50[a]	+	2,2,4-Trimethyl-1,3-pentadienol diisobutyrate	$C_{16}H_{30}O_4$	286.4070	16.391	309.2026	Up
51[a]	+	Oleoylcarnitine	$C_{25}H_{48}NO_4$	426.6610	16.407	426.3555	Down
52[a]	+	Eicosapentaenoic acid	$C_{20}H_{30}O_2$	302.4510	16.857	303.2297	Up
53[a]	+	LysoPC (20 : 5(5Z,8Z,11Z,14Z,17Z)/0 : 0)	$C_{28}H_{48}NO_7P$	541.6570	17.747	542.3217	Up
54[a]	+	LysoPC (18 : 2(9Z,12Z)/0 : 0)	$C_{26}H_{50}NO_7P$	519.6515	17.767	520.3379	Down
55[a]	+	LysoPC (16 : 0)	$C_{24}H_{50}NO_7P$	495.6301	18.443	496.3388	Down
56[a]	+	LysoPC (18 : 1(9Z)/0 : 0)	$C_{26}H_{52}NO_7P$	521.6673	18.996	544.3343	Down
57[a]	+	LysoPC (18 : 0)	$C_{26}H_{54}NO_7P$	523.6832	21.275	524.3693	Down

*Metabolites were matched by standards; [a]metabolites were confirmed by MS/MS fragmentation.

BAs are the final products of cholesterol breakdown and are primarily regulated by farnesoid X receptor (FXR) and G protein-coupled BA receptor 1 (GPBAR1, TGR5) to modulate their various functions [33]. The activation of intestinal FXR can reduce inflammation and immune cell infiltration and decrease intestinal epithelial permeability. Inflammation disrupts the metabolic balance between gut microbiota and BA, resulting in insufficient secondary BA production such as deoxycholic acid (DCA) and lithocholic acid, leading to reduced FXR activity and ineffective control of intestinal inflammation, which accelerates inflammation progression and carcinogenesis. However, excessive secondary BAs, especially DCA, can cause DNA damage by producing reactive oxygen species, promoting cell proliferation, reducing apoptosis and differentiation, and promoting the development of CRC [34]. Additionally, conjugated BA such as taurocholic acid (TCA) and glycocholic acid can have pro-inflammatory and anti-inflammatory effects by activating M1 and M2 macrophage receptor TGR5, respectively. Dysbiosis can disrupt conjugated BA and alter the pro-inflammatory and anti-inflammatory activities mediated by TGR5, causing intestinal damage. Metabolomics analysis results showed that SJE affected BA metabolism by modulating cholic acid, TCA, and DCA and was also one of the pathways that inhibited UC-to-CAC development.

Omega-3 polyunsaturated fatty acids such as alpha-linolenic acid, eicosapentaenoic acid, and docosahexaenoic acid (DHA) can usually reduce the inflammatory process and lower the risk of cancer [35]. The human body is unable to synthesize alpha-linolenic acid endogenously, and the conversion rate of DHA is extremely low; supplementation with stearic acid can improve the conversion rate of DHA [36]. Our previous analysis of the composition of SJE and literature research [37] found that SJE contained alpha-linolenic acid and stearic acid. It was hypothesized that SJE might be used as an omega-3 supplement to regulate lipid metabolism and play a role in preventing inflammation and cancer. SJE also contains LA, which is a synthetic precursor of AA and can inhibit inflammation by reducing the production of inflammatory factors such as TNF-α and IL-1 [38]. Recent studies have shown that LA is a major positive regulator of $CD8^+$ T-cell function, improves $CD8^+$ T-cell function and memory differentiation through mitochondrial reprogramming, prevents $CD8^+$ T-cell exhaustion, and enhances antitumor responses [39]. Moreover, the UC and CAC models caused abnormal levels of LPCs closely related to inflammation metabolism, mainly involving glycerophospholipid metabolism. Glycerophospholipids are the major lipid components of cell membranes, and alterations in glycerophospholipid metabolic pathways affect various cellular functions, such as membrane fusion and vesicular transport [40]. High concentrations of LPCs can impair intestinal barrier function and increase gastrointestinal permeability [41]. The levels of LPCs in mice tended to return to normal after the administration of SJE. Maoqing Wang et al. [42] identified five biomarkers of CRC, including LysoPC (14 : 0), LysoPC (16 : 0), LysoPC (18 : 0), LA, and tryptophan, through metabolomics studies. In this study, we found that LysoPC (16 : 0), LysoPC (18 : 0), LA, and tryptophan were all significantly regulated by SJE, providing supporting evidence for the effectiveness of SJE.

5. Conclusions

This study was novel in integrating validation experiments and metabolomics data to explore the protective effect of SJE on CAC. Combining UC experiments, we discussed the potential pathways for SJE to inhibit UC-to-CAC development at the organismal metabolomics level. SJE exhibited good activity in reversing DSS-induced UC and AOM/DSS-induced CAC, significantly alleviated symptoms such as blood in the stool, colon shortening, inflammatory response, and intestinal tissue damage in the model mice and regulated 57 differential metabolites common to both UC and CAC, which might inhibit the progression of UC to CAC by regulating lipid metabolism. Although dietary intake in daily life is not a substitute for medication, nutritional intervention is also a good way to alleviate symptoms and maintain intestinal health. This study may contribute to the development and rational application of functional foods from *Sophora japonica*, as well as to the prevention and treatment of UC and CAC.

Data Availability

All data used to support the findings of this study are presented in this paper. However, additional information can be obtained from corresponding author.

Conflicts of Interest

The authors declare no conflicts of interest.

Authors' Contributions

Funding acquisition and study design were done by Xiansheng Meng; study design, data processing, and writing the original draft were done by Ying Zheng; pharmacodynamic experiments were carried out by Tianjiao Li, Hao Yu, and Li-ying Han; index assays were done by Xi Luo and Mengnan Jia; reviewing and editing were done by Shuai Wang and Yongrui Bao. All authors have read and agreed to the published version of the manuscript.

Acknowledgments

This research was funded by grants from the Key R&D Projects in Liaoning Province (2020JH2/10300088) and the Basic Research Project of Liaoning Provincial Department of Education (JYTQN2023474).

Supplementary Materials

Figure S1: PLS-DA analysis of all samples. PLS-DA plots of all samples from UC experiments in negative ion mode (A) and positive ion mode (B). PLS-DA plots of all samples from CAC experiments in negative ion mode (C) and positive ion mode (D). Table S1: Scoring criteria for pathological states of UC; Table S2: Scoring criteria for pathological states of CAC. (*Supplementary Materials*)

References

[1] S. C. Ng, H. Y. Shi, N. Hamidi et al., "Worldwide incidence and prevalence of inflammatory bowel disease in the 21st century: a systematic review of population-based studies," *The Lancet*, vol. 390, no. 10114, pp. 2769–2778, 2017.

[2] S. C. Shah and S. H. Itzkowitz, "Colorectal cancer in inflammatory bowel disease: mechanisms and management," *Gastroenterology*, vol. 162, no. 3, pp. 715–730.e3, 2022.

[3] M. C. Fantini and I. Guadagni, "From inflammation to colitis-associated colorectal cancer in inflammatory bowel disease: patho-genesis and impact of current therapies," *Digestive and Liver Disease*, vol. 53, no. 5, pp. 558–565, 2021.

[4] Q. Tang, S. Cang, J. Jiao et al., "Integrated study of metabolomics and gut metabolic activity from ulcerative colitis to colorectal cancer: the combined action of disordered gut microbiota and linoleic acid metabolic pathway might fuel cancer," *Journal of Chromatography A*, vol. 1629, Article ID 461503, 2020.

[5] J. Burisch and P. Munkholm, "The epidemiology of inflammatory bowel disease," *Scandinavian Journal of Gastroenterology*, vol. 50, no. 8, pp. 942–951, 2015.

[6] M. Yashiro, "Ulcerative colitis-associated colorectal cancer," *World Journal of Gastroenterology*, vol. 20, no. 44, pp. 16389–16397, 2014.

[7] Y. Liu, B. G. Li, Y. H. Su et al., "Potential activity of traditional Chinese medicine against ulcerative colitis: a review," *Journal of Ethnopharmacology*, vol. 289, no. 2022, Article ID 115084, 2022.

[8] J. Wu, Y. Luo, Y. Shen et al., "Integrated metabonomics and network pharmacology to reveal the action mechanism effect of Shaoyao Decoction on ulcerative colitis," *Drug Design, Development and Therapy*, vol. 16, pp. 3739–3776, 2022.

[9] Y. Zheng, C. Liang, Z. Li et al., "Study on the mechanism of Huangqin Decoction on rats with ulcerative colitis of damp-heat type base on mtDNA, TLR4, p-PI3K, p-Akt protein expression and microbiota," *Journal of Ethnopharmacology*, vol. 295, Article ID 115356, 2022.

[10] X. He, Y. Bai, Z. Zhao et al., "Local and traditional uses, phytochemistry, and pharmacology of Sophora japonica L.: a review," *Journal of Ethnopharmacology*, vol. 187, pp. 160–182, 2016.

[11] Y. Kim, Y. Oh, H. Lee et al., "Prediction of the therapeutic mechanism responsible for the effects of Sophora japonica flower buds on contact dermatitis by network-based pharmacological analysis," *Journal of Ethnopharmacology*, vol. 271, Article ID 113843, 2021.

[12] Y. Liu, W. Huang, S. Ji, J. Wang, J. Luo, and B. Lu, "Sophora japonica flowers and their main phytochemical, rutin, regulate chemically induced murine colitis in association with targeting the NF-κB signaling pathway and gut microbiota," *Food Chemistry*, vol. 393, no. 2022, Article ID 133395, 2022.

[13] A. Elberry, S. Mufti, J. Al-Maghrabi et al., "The protective effect of Sophora japonica on prostatic hypertrophy and inflammation in rat," *Inflammopharmacology*, vol. 28, no. 6, pp. 1525–1536, 2020.

[14] T. Wang, M. Miao, M. Bai et al., "Effect of sophora japonica total flavonoids on pancreas, kidney tissue morphology of streptozotocin-induced diabetic mice model," *Saudi Journal of Biological Sciences*, vol. 24, no. 3, pp. 741–747, 2017.

[15] H. S. Seo, K. H. Kim, D. Y. Kim et al., "GC/MS analysis of high-performance liquid chromatography fractions from Sophora flavescens and Torilis japonica extracts and their in vitro anti-neosporal effects on Neospora caninum," *Journal of Veterinary Science*, vol. 14, no. 3, pp. 241–248, 2013.

[16] Y. Zhu, W. Wang, R. Ruan, and J. Chen, "Oxidative potential and nanoantioxidant activity of flavonoids and phenolic acids in Sophora flavescens," *International Journal of Analytical Chemistry*, vol. 2022, Article ID 4601350, 7 pages, 2022.

[17] S. Jiang, D. Song, H. Zhao et al., "Bioactivity and component analysis of water extract of Sophora japonica against hyperuricemia by inhibiting xanthine oxidase activity," *Foods*, vol. 11, no. 23, p. 3772, 2022.

[18] Q. Wang, Y. Li, K. W. Li, and C. Z. Zhou, "Sophoridine: a review of its pharmacology, pharmacokinetics and toxicity," *Phytomedicine*, vol. 95, no. 2022, Article ID 153756, 2022.

[19] S. S. Bhat, S. K. Prasad, C. Shivamallu et al., "Genistein: a potent anti-breast cancer agent," *Current Issues in Molecular Biology*, vol. 43, no. 3, pp. 1502–1517, 2021.

[20] M. Imran, A. Rauf, T. Abu-Izneid et al., "Luteolin, a flavonoid, as an anticancer agent: a review," *Biomedicine and Pharmacotherapy*, vol. 112, Article ID 108612, 2019.

[21] M. Reyes-Farias and C. Carrasco-Pozo, "The anti-cancer effect of quercetin: molecular implications in cancer metabolism," *International Journal of Molecular Sciences*, vol. 20, no. 13, p. 3177, 2019.

[22] S. Muthusami, I. K. Ramachandran, K. N. Babu et al., "Role of inflammation in the development of colorectal cancer," *Endocrine, Metabolic & Immune Disorders- Drug Targets*, vol. 21, no. 1, pp. 77–90, 2021.

[23] D. D. Eichele and K. K. Kharbanda, "Dextran sodium sulfate colitis murine model: an indispensable tool for advancing our understanding of inflammatory bowel diseases pathogenesis," *World Journal of Gastroenterology*, vol. 23, no. 33, pp. 6016–6029, 2017.

[24] X. Hua, R. C. Ungaro, L. M. Petrick et al., "Inflammatory bowel disease is associated with prediagnostic perturbances in metabolic pathways," *Gastroenterology*, vol. 164, no. 1, pp. 147–150.e2, 2023.

[25] A. Gold, F. Choueiry, N. Jin, X. Mo, and J. Zhu, "The application of metabolomics in recent colorectal cancer studies: a state-of-the-art review," *Cancers*, vol. 14, no. 3, p. 725, 2022.

[26] C. Li, Y. Wang, D. Liu et al., "Squalene epoxidase drives cancer cell proliferation and promotes gut dysbiosis to accelerate colorectal carcinogenesis," *Gut*, vol. 71, no. 11, pp. 2253–2265, 2022.

[27] X. Bian, R. Liu, Y. Meng, D. Xing, D. Xu, and Z. Lu, "Lipid metabolism and cancer," *Journal of Experimental Medicine*, vol. 218, no. 1, Article ID e20201606, 2021.

[28] E. Piccinin, M. Cariello, and A. Moschetta, "Lipid metabolism in colon cancer: role of liver X receptor (LXR) and stearoyl-CoA desaturase 1 (SCD1)," *Molecular Aspects of Medicine*, vol. 78, Article ID 100933, 2021.

[29] J. D. Imig, "Eicosanoid blood vessel regulation in physiological and pathological states," *Clinical Science*, vol. 134, no. 20, pp. 2707–2727, 2020.

[30] A. Yamaguchi, E. Botta, and M. Holinstat, "Eicosanoids in inflammation in the blood and the vessel," *Frontiers in Pharmacology*, vol. 13, Article ID 997403, 2022.

[31] S. Dhall, D. S. Wijesinghe, Z. A. Karim et al., "Arachidonic acid-derived signaling lipids and functions in impaired healing," *Wound Repair and Regeneration*, vol. 23, no. 5, pp. 644–656, 2015.

[32] A. Mohammed and R. H. Shoemaker, "Targeting the leukotriene pathway for colon cancer interception," *Cancer Prevention Research*, vol. 15, no. 10, pp. 637–640, 2022.

[33] L. Chen, T. Jiao, W. Liu et al., "Hepatic cytochrome P450 8B1 and cholic acid potentiate intestinal epithelial injury in colitis by suppressing intestinal stem cell renewal," *Cell Stem Cell*, vol. 29, no. 9, pp. 1366–1381.e9, 2022.

[34] W. Jia, G. Xie, and W. Jia, "Bile acid-microbiota crosstalk in gastrointestinal inflammation and carcinogenesis," *Nature Reviews Gastroenterology and Hepatology*, vol. 15, no. 2, pp. 111–128, 2018.

[35] M. Liu, Z. Wang, X. Liu et al., "Therapeutic effect of Yiyi Fuzi Baijiang formula on TNBS-induced ulcerative colitis via metabolism and Th17/Treg cell balance," *Journal of Ethnopharmacology*, vol. 309, no. 2023, Article ID 116301, 2023.

[36] S. D'Angelo, M. L. Motti, and R. Meccariello, "ω-3 and ω-6 polyunsaturated fatty acids, obesity and cancer," *Nutrients*, vol. 12, no. 9, p. 2751, 2020.

[37] J. Tian, Y. Gong, and J. Li, "Nutritional attributes and phenolic composition of flower and bud of Sophora japonica L. and Robinia pseudoacacia L," *Molecules*, vol. 27, no. 24, p. 8932, 2022.

[38] B. Zhou, J. Liu, Y. Wang et al., "Protective effect of ethyl rosmarinate against ulcerative colitis in mice based on untargeted metabolomics," *International Journal of Molecular Sciences*, vol. 23, no. 3, p. 1256, 2022.

[39] C. B. Nava Lauson, S. Tiberti, P. A. Corsetto et al., "Linoleic acid potentiates CD8+ T cell metabolic fitness and antitumor immunity," *Cell Metabolism*, vol. 35, no. 4, pp. 633–650.e9, 2023.

[40] W. Zheng, J. Jia, C. Zhang, P. Zhang, S. Song, and C. Ai, "Undaria pinnatifida fucoidan ameliorates dietary fiber deficiency-induced inflammation and lipid abnormality by modulating mucosal microbiota and protecting intestinal barrier integrity," *International Journal of Biological Macromolecules*, vol. 247, no. 2023, Article ID 125724, 2023.

[41] M. T. Snaebjornsson, S. Janaki-Raman, and A. Schulze, "Greasing the wheels of the cancer machine: the role of lipid metabolism in cancer," *Cell Metabolism*, vol. 31, no. 1, pp. 62–76, 2020.

[42] M. Wang, Z. Long, W. Xue et al., "Discovery of plasma biomarkers for colorectal cancer diagnosis via untargeted and targeted quantitative metabolomics," *Clinical and Translational Medicine*, vol. 12, no. 4, p. e805, 2022.